Optical Properties I

Experimental Determination of the Phonon-Eigenvector of Silicon Carbide by Raman Spectroscopy
B. Herzog, S. Rohmfeld, M. Hundhausen, L. Ley, K. Semmelroth, G. Pensl
Universität Erlangen-Nürnberg, Germany

Raman Microprobe Study of Carrier Density Profiles in Modulation-Doped 6H-SiC
S. Nakashima[1,2], Y. Nakatake[2], Y. Yano[2], N. Ohtani[3], M. Katuno[3]
[1]National Institute of Advanced Industrial Science and Technology, Japan; [2]Miyazaki University, Japan; [3]Nippon Steel Co. Ltd., Japan

A Raman Study on Metal-SiC Interface Reactions
E. Kurimoto[1], H. Harima[2], T. Toda[3], M. Sawada[3], S. Nakashima[4], M. Iwami[5]
[1]Osaka University, Japan; [2]Kyoto Institute of Technology, Japan; [3]SANYO Electric Co., Japan; [4]AIST, Japan; [5]Okayama University, Japan

Optical, Surface and Interface Properties of Ion Implanted 4H-SiC Epi-structures
Z. C. Feng[1], W. Y. Chang[2], J. Lin[2], F. Yan[3], Y. M. Zhang[3], J. H. Zhao[3]
[1]Axcel Photonics, USA; [2]National University of Singapore, Singapore; [3]Rutgers University, USA

Raman Scattering from Wurtzite GaN Bulk Crystal
P. Verma, M. Yamada
Kyoto Institute of Technology, Japan

Characterization of SiC Band-Edge Absorption Properties by Free-Carrier Absorption Technique with Variable Excitation Spectrum
P. Grivickas[1], V. Grivickas[2], A.Galeckas[1,2], J.Linnros[1]
[1]Royal Institute of Technology, Sweden; [2]Vilnius University, Lithuania

Experimental Determination of the Phonon-Eigenvectors of Silicon Carbide by Raman Spectroscopy

B. Herzog, S. Rohmfeld, M. Hundhausen, and L. Ley
Institut für Technische Physik, Friedrich-Alexander Universität Erlangen-Nürnberg
Erwin-Rommel-Straße 1, D-91058 Erlangen, Germany
Phone: (49) 9131 8527259, FAX: (49) 9131 8527889
e-mail: Martin.Hundhausen@physik.uni-erlangen.de
K. Semmelroth and G. Pensl
Institut für Angewandte Physik, Friedrich-Alexander Universität Erlangen-Nürnberg

The phonon frequencies of silicon carbide (SiC) depend on the atomic masses of the constituent elements Si and C. In general, the frequency decreases, when the mass of one kind of atom is increased by isotopic substitution. Quantitatively, the frequency shift $\Delta\omega(\vec{q})$ of a phonon mode of wave vector $\vec{q}$ depends on how much of the energy contained in that mode is carried by the sublattice of substituted atoms. This energy is proportional to the square of the phonon eigenvector $|e_i|$ according to [1]:

$$\frac{\Delta\omega(q)}{\omega(q)} = \frac{\Delta M_i}{2M_i} |e_i(q)|^2 , \qquad (1)$$

where $\Delta M_i/M_i$ is the relative mass change of element i. By measuring $\Delta\omega(q)$ one is thus in the position to determine $|e_i(q)|$ for one of the sublattices (C or Si).
We have grown 6H-, 4H-, and 15R-SiC polytypes enriched to 83% with the ^{13}C-isotope. The frequencies of all Raman active phonon modes have been measured accurately in back-scattering geometry along the c-axis direction.
The absolute values of the carbon eigenvector e_C for the transversal and longitudinal branches as a function of the phonon wave vector q evaluated with Eq. 1 are shown in Figs. 1 and 2, respectively. For these figures, the large Brillouin zone of 3C-SiC has been used and the observed phonon modes of the different SiC polytypes are plotted with q-vectors assigned by use of the zone folding concept[2]. The experimental data are compared to eigenvectors calculated with a linear chain model employing the force constants given in the literature[2,3]. Good agreement is observed for the transversal modes in Fig. 1, whereas there are larger deviations for the longitudinal modes. We discuss these deviations that are most probably due to deficiencies in the values of the force constants used in Ref. [3].

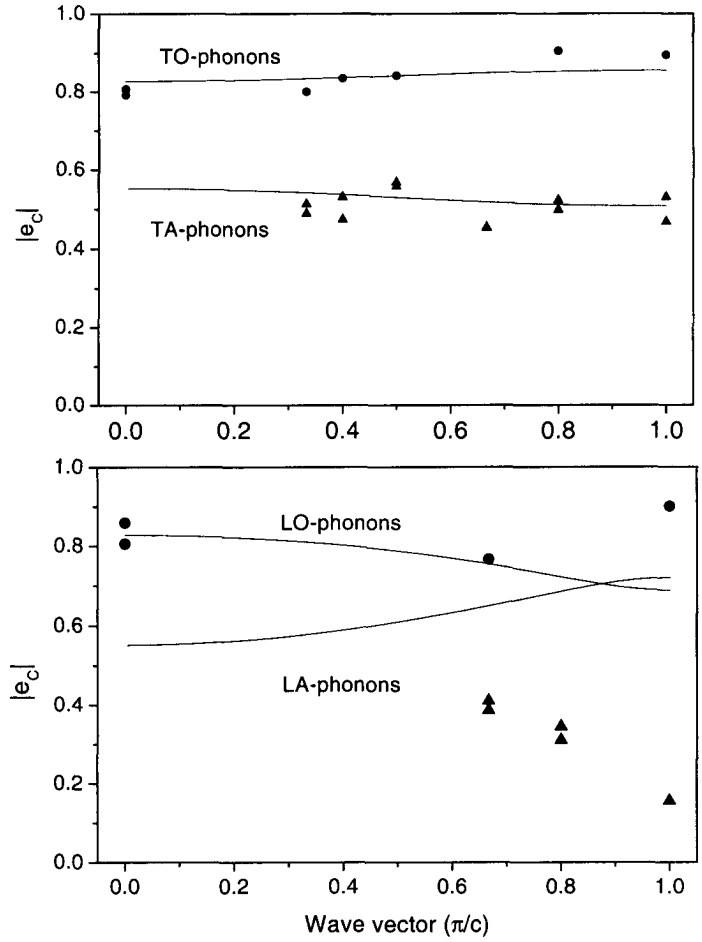

Fig.1: Absolute values of the phonon eigenvector $|e_C(q)|$ of carbon atoms for the transversal modes as derived from the isotope shift of Raman frequencies. Circles: TO-modes, triangles: TA-modes. Lines are calculated with a linear chain model according to [2].

Fig.2: Absolute values of the phonon eigenvector $|e_C(q)|$ of carbon atoms for the longitudinal modes as derived from the isotope shift of Raman frequencies. Circles: LO-modes, triangles: LA-modes. Lines are calculated with a linear chain model according to[3].

[1] F. Widulle, T. Ruf, O. Buresch, A. Debernardi, and M. Cardona, Phys. Rev. Lett. **82**, 3089 (1999).
[2] S. Nakashima, K. Tahara, Phys. Rev. B **40**, 6339 (1989).
[3] S. Nakashima, H. Harima, T. Tomita, and T. Suemoto, Phys. Rev. B **62**, 16605 (2000).

Raman Microprobe Study of Carrier Density Profiles in Modulation-doped 6H-SiC.

S.Nakashima,[1,2] ,Y.Nakatake[2], Y.Yano[2], H.Harima[3] , N.Ohrani[4] and M.Katsuno[4]

[1]Power Electronics Research Center, AIST, R & D Association for Future Electron Devices, 1-1-1 Umezono, Tsukuba, Ibaraki, 305-8568, Japan

[2]Deparment of Electrical and Electronics Engineering, Miyazaki University, 1-1Gakuen Kibanadai Nishi, Miyazaki 889-2192, Japan

[3]Faculity of Engineering & Design, Kyoto Instoytute of Technology, Matsgasaki Goshokaido-tyou, Kyoto 606-8585, Japan

[4]Advanced Technology Research Laboratories, Nippon Steel Co. Ltd, 20-1Shintomi, Futtsu, Chiba 293-8511, Japan

Electrical properties such as carrier concentration and mobility of semiconductors have mainly been studied by Hall and C-V measurements so far. Recent studies have demonstrated that the Raman spectroscopy can also be used to characterize the electrical properties of polar semiconductors[1,2]. Raman microprobe measurement has a great advantage for characterization of the electrical properties of local areas on the micron meter scale, because it is non destructive and contactless technique. Up to now the Raman microprobe has been applied to determination of carrier density profiles of GaP diode [3], SiC wafers[4] and around micropipes in SiC [5] .

In this work we have measured Raman images for LO-phonon plasmon coupled mode (LOPCM) in modulation doped 6HSiC crystals and determined spatial distribution of N-donors. From the analysis of the Raman profile the dependence of the carrier mobility on the impurity concentration and the residence time of the N_2 dopant gas on the surface of growing crystals after switch-off of the doping gas are inferred. The residence time thus inferred is in agreement with that estimated from the test of the furnace system.

6H SiC crystals were grown by modified-Lely method. Modulation doping was made by on-off switch of the N_2 gas [6] so that the doped impurity has a step -like distribution as shown in Fig.1(a). The surface of the sample used is (0001). Raman spectra were measured using a triple spectrometer (f=0.6 m) with an image expander of 2 magnification and a cooled CCD detector. One-dimensional images of the LOPCM were obtained using an optical microscope. Laser beam was linearly expanded with a cylindrical lens and illuminated on the sample surfaces.

The measured line shape of the LOPCM was fitted to the theoretical curve using carrier concentration (n) and mobility (μ) as adjustable parameters[7]. The carrier concentration thus determined is plotted as a function of the distance in Fig.1(b). The carrier concentration rises steeply after

the dopant-gas supply and decreases slowly after the stop of the gas. The transition region between the doped and undoped zones is ~20 μm in the switch-off case and ~8μm in the switch-on case. This result indicates that N_2 gas remains for a while after the stop of the dopant-gas supply. The residence time of N_2 gas on surface of the growing crystals inferred from the width of the transition region and the growth rate (1mm / h) is 74 s, which is in close agreement with that (75 s) determined in advance from the test of the growth furnace. The relationship between the carrier mobility and concentration is also obtained by the line shape analysis of the LOPCM.

The above results demonstrate that Raman microprobe imaging is useful to analyze the doping process of impurity in bulk and epitaxial SiC.

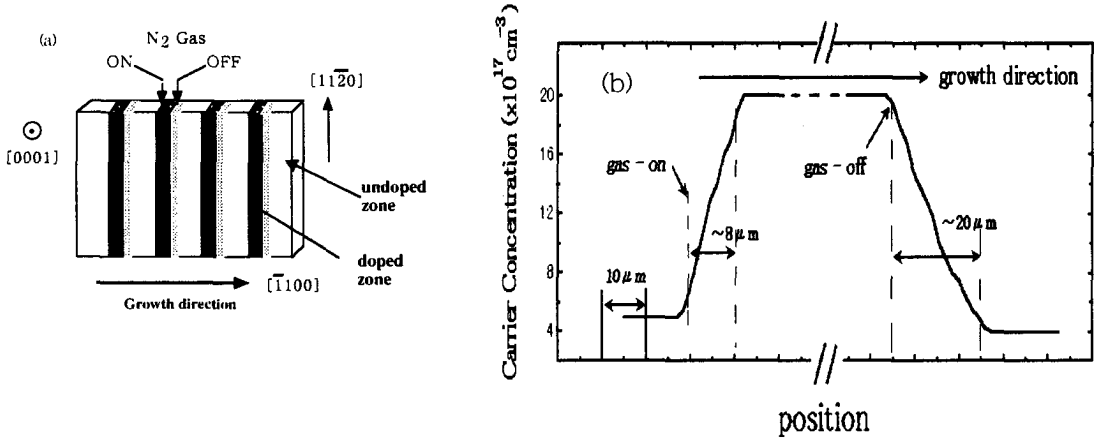

Fig.1 (a) Schematic structure of modulation-doped SiC and (b) profile of the carrier concentration determined from the Raman analysis.

References

[1] S. Nakashima and M.Han gyo, IEEE J Quantum Electronics, **25**, 965 (1989)

[2] S. Nakashima and H. Harima, phys. stat. sol. **162** (a) 39 (1997)

[3] S.Nakashima, H.Yugami, A.Fujii, M.Hangyo and H. Yamanaka, J.Appl.Phs., **64**, 3067(1988)

[4] H. Harima, S. Nakashima and T. Uemura, J. Appl. Phys. **78**, 1996(1995).

[5] J.C. Burton, L/Sun, M.Pophristic, S.J. Lukacs, F.H.Long, Z.C.Feng and I.T.Ferguson, J.Appl.Phys.84, 6268(1998)

[6]M.Katsuno,N..Ohtani, J.Takahashi, H.Yashiro and M.Kanaya, Jpn.J.Appl.Phys. 38,4661(1999)

[7]H.Harima, T.Hosoda and S.Nakashima, Material Science Forum,338-342,603(2000)

A Raman Study on Metal-SiC Interface Reactions

E. Kurimoto[1], H. Harima[2], T. Toda[3], M. Sawada[3], S. Nakashima[4], M. Iwami[5]

[1] Dept. Applied Physics, Osaka Univ., Osaka 565-0871, Japan
[Tel: +81-6-6879-7854, Fax: +81-6-6879-7856, e-mail:eiji@ap.eng.osaka-u.ac.jp]
[2] Dept. Elecronics and Information Science, Kyoto Institute of Technology, Kyoto 606-8585, Japan
[3] Optoelectonics Devices Dept., SANYO Electric Co., Hirakata, Osaka 573-8534, Japan
[4] Power Electronics Research Center, AIST, Tsukuba, Ibaraki 305-8568, Japan
[5] Research Laboratory for Surface Science, Okayama Univ., Okayama 700-8530, Japan

An important problem for fabricating variety of SiC-based electronic devices is to find suitable electrode materials with their processing technique to obtain low-resistance (ohmic) contacts with SiC layers. Obviously, the contact resistance depends on the electrode-SiC interface reactions. Therefore, in order to reveal the mechanisms for lowering the contact resistance, it is crucial to probe the interface reactions at various processing conditions.

A common method for this purpose is bombarding charged particles to extract relative abundance of constituent elements; i.e., Auger-electron spectroscopy (AES), secondary ion mass spectrometry (SIMS), and Rutherford back scattering (RBS). These methods are, however, all destructive, expensive, and sometimes very time-consuming. We would like to propose here a Raman scattering technique that provides an easy test for interface reactions. It is an optical method, therefore, non-destructive, and enables 2-dimensional analysis with micrometer resolution, which is suitable for diagnosis of future integrated circuits.

Here we selected Ti or Ni as a standard electrode material. The metallic layer was deposited in vacuum on 6H-SiC commercial wafers (both sides polished). Both Si- and C-faces were tested for deposition, changing the metallic-layer width, annealing gas species (N_2 or Ar), temperature (500-1100°C) and time. The Raman spectra were observed at room temperature by back scattering using a microscope. The Ar^+ laser line at 5145 Å was used for excitation. Figure 1 shows a typical result for Ti/SiC, annealed in Ar at 1000°C for 5 min.

Here, (a) shows a result when Ti was deposited on SiC (C-face), and the probe laser was focused on the electrode top surface, while (c) was observed when the probe laser was focused through the SiC layer on the Ti/SiC interface. The spectrum (b) was obtained like (c), but the Si-face was selected for Ti-deposition. The optical arrangement like (b) or (c) is possible because of the large band gap nature of SiC, which is an important advantage in our optical detection as mentioned below. The common sharp peaks in (b) and (c) are phonon signals of SiC. Figure 1 shows distinctly different features depending on the observed portions; (a) is dominated by broad peaks for TiC_{1-x}, while (c), enhanced in scale in Fig.2, shows faint but sharp structures ascribed to $TiSi_2$. Contrary to (c), Ti/SiC (Si-face) interface shows strong TiO_2 signals as depicted in Fig.1 (b).

These results show various findings for this annealing condition; First, decomposition of SiC is enhanced at the C-face, which promotes Ti-silicidation reaction. On the contrary, Ti-oxidation due to inevitable oxygen impurities incorporated in the annealing process is promoted on the Si-face. Second, carbon atoms reach the top surface of electrode by thermal diffusion, which reflects superior diffusivity of carbon atoms than Si in Ti.

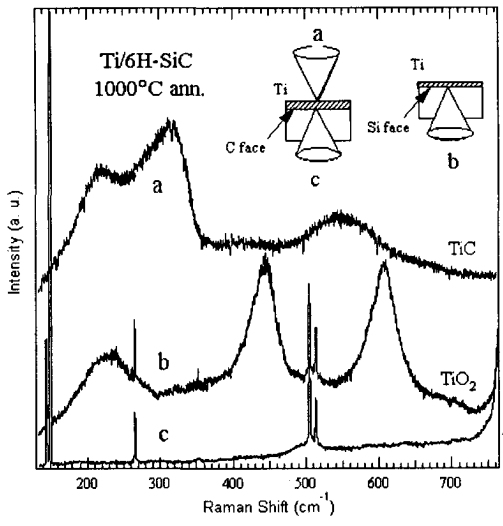

Fig.1 Typical Spectra

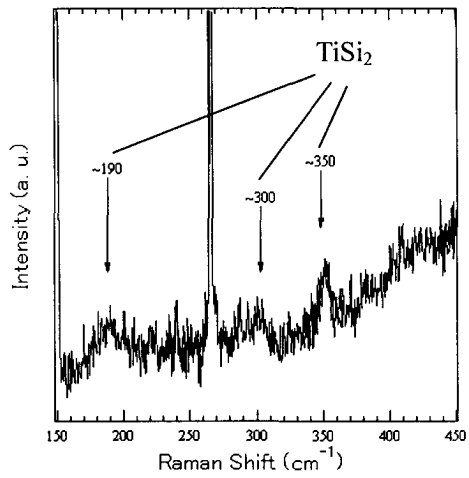

Fig.2 Spectrum Fig.1 (c) is enhanced.

Optical, surface and interface properties of ion implanted 4H-SiC

Z. C. Feng,* W. Y. Chang,+ J. Lin,+ F. Yan,# and J. H. Zhao#

*Axcel Photonics Inc., 45 Bartlett Street, Marlborough, MA 01752, USA.
{tel: 1-508-481-9200, fax: 1-508-481-9261, e-mail: zfeng@axcelphotonics.com}
+Department of Physics, National University of Singapore, 119260 Singapore
#Department of Elect. & Computer Engi., Rutgers University, Piscataway, NJ 08855, USA

A series of Al ion-implanted and C^+-Al^+ co-implanted 4H-SiC epilayers have been studied by optical transmission (OT), micro-Raman scattering and Fourier transform infrared (FTIR) spectroscopy measurements. The damage and amorphization of SiC layer by ion-implantation, and the elimination or suppression of the implantation induced amorphous layer via high temperature annealing are evidenced. The recovery of the crystallinity and the activation of the implant acceptors are confirmed.

SiC is a promising material for electronic and optoelectronic devices operating in high temperature, high power and other extreme environments. In recent years, much progress has been made in the research and development of 6H- and 4H-SiC materials and devices, for which, a critical issue is the doping technique. It is limited to use conventional diffusion methods to produce the SiC-based p-n junction and devices due to the very low thermal diffusion coefficient. The ion implantation into SiC appears to be the primary method to produce selective structured p-doped layers. Al is a preferred acceptor in SiC due to its lower activation (ionization) energy (0.24 eV). In order to improve the efficiency of Al^+ to substitute Si atom sites, co-implantation of C ions is expected to enhance to break the balance of stochiometry towards C enrichment and thus improve the chance of Al dopants to settle at Si atom sites. Ion implantation can cause severe damage of the crystallinity. Post-annealing is necessary for crystal recovery and electrical activation of implanted species. In this paper, investigation is focused to analyze the effects of Al^+ and C^+-Al^+ implanted/annealed 4H-SiC, and to establish the correlation of their optical, surface and interface properties with process.

Experimental samples are epitaxially grown n^-/n^+ 4H-SiC/4H-SiC. Multiple-energy implantation, 65-196 KeV for Al ions and 32-160 KeV for C ions, at room temperature (RT), were carried out to obtain a box-like implantation profile. C ions were implanted preceding Al ions. Annealing in an ultrahigh purity Argon ambient in a conventional furnace was performed at 1550 °C for 30 min. By means of UV-Visible OT, micro-Raman and FTIR spectroscopy, the surface and subsurface modifications induced by ion implantation and post-annealing are examined.

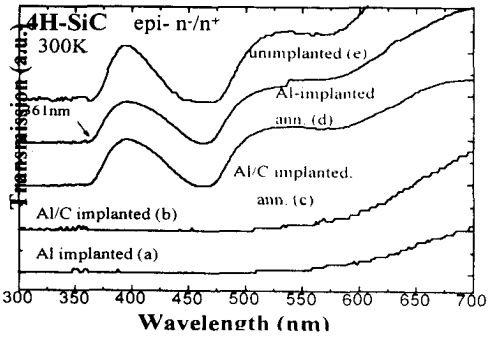

Fig. 1 OT spectra recorded on as-implanted (a)-(b), post-implantation annealed (c)-(d), and one virgin (e) 4H-SiC.

Fig. 1 shows optical transmission spectra, indicating the damage and amorphization of SiC layer by ion-implantation, for Al^+ implanted, in (a), and Al^+/C^+ co-implanted, in (b), samples. After 1550°C annealing, a sharp transition edge near 360 nm (3.4 eV) appears, as shown in (c) and (d). It presents the optical absorption gap of crystalline 4H-SiC, in comparison with

the OT spectrum from a virgin sample, in (e). Therefore the elimination or suppression of the implantation induced amorphous layer via high temperature (HT) annealing is evidenced.

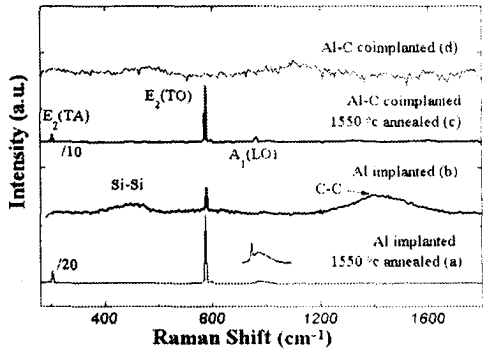

Fig. 2 Comparative Raman scattering for implanted and annealed 4H-SiC.

Fig. 2 shows micro-Raman measurements on four samples. It is seen that after Al^+ implantation at RT, only weak peaks and two broad bands are observable. These broad bands at ~500 cm^{-1} and 1400 cm^{-1} are typical for amorphous SiC, indicating the damage of 4H-SiC crystallinity and the formation of an amorphous phase. After HT annealing, Raman spectra close to that of crystalline 4H-SiC appear, predicting the recovery of the SiC crystalline structure.

Figure 3 exhibits the IR reflectance for four implanted samples and a virgin (un-implanted) one. Significant variations are seen after both Al/C and Al implantation, comparing with the un-implanted one, especially in reststrahlen band: the intensity decreases greatly; one notch at 934 cm^{-1}, with the minimum as low as 30%, becomes a dominant feature in the reststrahlen band. However, HT annealing recovered the optical behaviour, both in intensity and line shape, but in different degree.

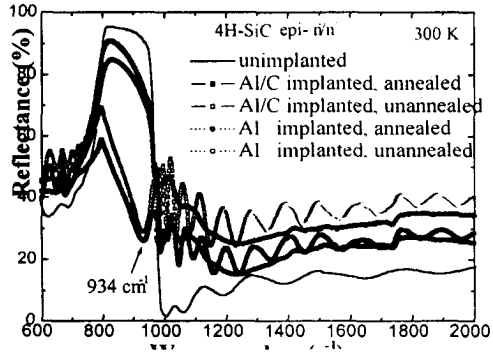

Figure 3 IR reflectance spectra from Al^+ and C^+/Al^+ implanted/annealed n-/n+ epitaxial 4H-SiC, and an unimplanted sample for comparison.

To explain these experimental findings, we have developed a multiple-layered model and applied to the reflectance profiles. Samples are defined as three-layer structural matrix in the configuration of amorphous layer/crystalline 4H-SiC/substrate. For amorphous SiC, the Si-C stretching mostly appears as a broad band in IR absorption, and it is treated as an adjustable parameter in the fitting process. The reststrahlen band can be fitted by the classical dispersion theory with proper choice of the dispersion parameters related to the materials properties.

Our detailed simulation and analysis have produced significant results. The notch at 934 cm^{-1} was found to originate from amorphous SiC, i.e. a continuous buried amorphous layer close the surface. The Si-C stretching frequency derived from fitting is at 780cm^{-1}, which is consistent with previous results in a-SiC:H films. The thickness of amorphized layer derived from FTIR fitting is about 0.32 μm for Al/C co-implanted and 0.35 μm for Al single implanted samples. After HT annealing, the structural matrix in the implanted region changes from amorphous phase into crystalline one with high carrier concentration. Acceptor activation is evidenced by the increase of the plasma frequency, ω_p, up to 600 cm^{-1} (corresponding to N=1.3x10^{19}cm^{-3}) after annealing. Better recovery of optical properties in Al/C co-implanted than Al single implanted sample is verified. The correlation is established between the observed variation of optical, surface and interface properties with the structural modifications induced by implantation and annealing. All these results indicate that high temperature annealing successfully refreshes the 4H-SiC crystallinity, even though the degree of recovery strongly depends on implantation conditions.

Raman scattering from wurtzite GaN bulk crystal

P. Verma and M. Yamada

Dept. of Electronics and Information Science, Kyoto Institute of Technology, Kyoto, Japan.
(E-mail: verma@dj.kit.ac.jp; Tel.: +81 75 724 7439; Fax: +81 75 724 7400)

GaN has long been considered as a promising material for semiconductor device applications due to its unique electronic and mechanical properties and has been the focus of intensive studies in the resent years. With a direct wide band-gap and high thermal stability, GaN is a suitable material for the blue and near-UV light emitting devices and high temperature electronics [1]. However, the major difficulty that has hindered GaN epilayer research and its commercial applications is the lack of a suitable substrate material that is lattice-matched and thermally compatible with GaN. Nevertheless, GaN has been grown commonly on SiC, ZnO and Al_2O_3. In fact, several other materials have also been used as the substrate, but the optical and electrical properties of the grown epilayers have not been satisfactory. GaN bulk material itself is the best choice as the substrate material, however, there has hardly been any success in the growth of good quality bulk GaN, which is mainly due to the high melting temperature of GaN and low reactivity between gallium and nitrogen. Moreover, in spite of the technological perspective of this material, only little work has been performed on the fundamental properties of GaN compared to the other III-V semiconductors, which is partly due to the unavailability of good GaN crystals. Under ambient conditions, GaN crystallizes in the hexagonal wurtzite (2H) structure with the space group C_{6v}^4. However, some epitaxial growths have also resulted in cubic zinc blend (3C) structures. The two structures basically differ in the stacking of the Ga-N bilayers perpendicular to the hexagonal [0001] and cubic [111] directions, respectively. Recently, there has been some success in the growth of large size 2H bulk GaN with good crystalline qualities. In this paper, we report, for the first time, some basic characterization of 2H bulk GaN crystal in a view to understand the fundamental vibronic and electric properties of this material, studied by polarization-dependent Raman

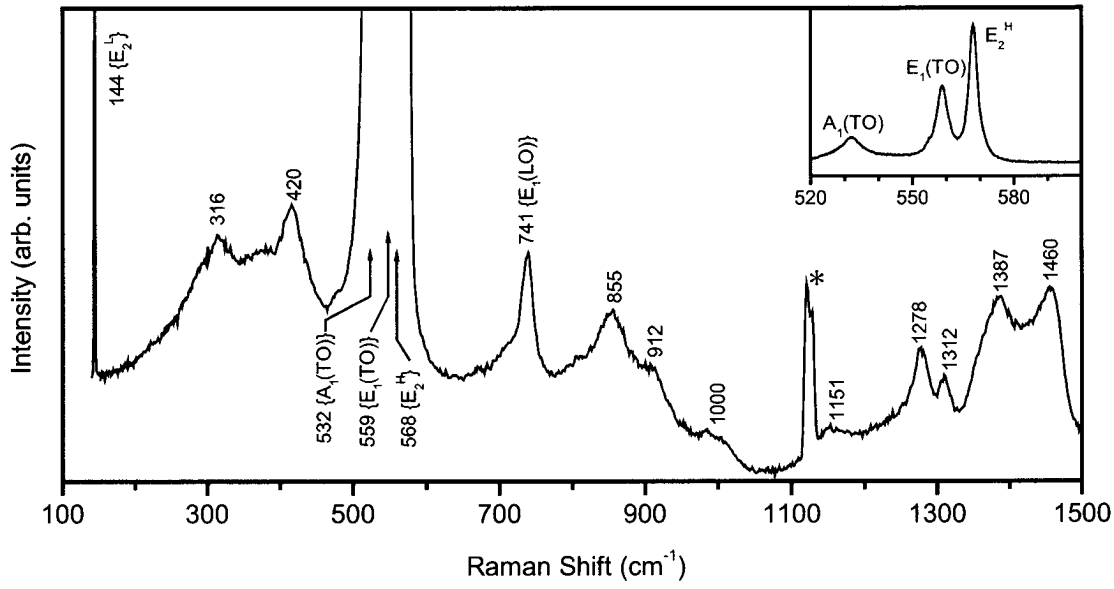

Fig. 1 Unpolarized room-temperature Raman spectrum from GaN bulk crystal in combined [x(y,y)-x + x(y,z)-x] backscattering configuration. The numbers indicate phonon frequencies in cm^{-1}. Inset shows the details of phonon modes between 520 and 580 cm^{-1}.

scattering technique under various scattering configurations. The as-grown GaN crystal was cut in to a 0.5 mm thick, 1 cm square-shaped wafer and was mirror polished for better scattering. Raman scattering studies were performed under various scattering configurations at room temperature. GaN is transparent to the probing laser wavelength (514.5 nm), which brings an advantage of large scattering volume, resulting in strong scattering intensities. Due to the momentum conservation, the first-order Raman spectrum shows phonons corresponding to the Γ-point ($k = 0$). In the wurtzite structure, the group theory predicts eight types of phonons, $2A_1$, $2E_1$, $2B_1$, and $2E_2$, out of which $1A_1$ and $1E_1$ modes are acoustic and the rest are optic. Depending upon the scattering configuration, all or some of these optic phonons along with various combination modes can be observed in a Raman spectrum. Taking the z direction along the c-axis, an unpolarized scattering in the backscattering geometry can be described by the combined configuration [x(y,y)-x + x(y,z)-x], where the symbols, from left to right, outside the bracket indicate the direction of incident and scattered light and inside bracket indicate the polarization direction of incident and scattered light, respectively. Figure 1 shows a Raman spectrum measured from bulk GaN crystal in the [x(y,y)-x + x(y,z)-x] scattering configuration. The details of phonon structures between 520 and 580 cm^{-1} are displayed in the inset. The LO modes in Raman spectrum have very weak intensity, which indicates that the sample has large charge carriers, which screen the LO phonons. Although a phonon-plasmon coupled mode could not be observed, it was otherwise confirmed that the sample has a charge carrier density of about 10^{18} cm^{-3}. The low-frequency E_2 mode shows fairly small line width, indicating long lifetime. We could not observe the B_1 modes in our experiments, probably due to their weak intensities. Figure 1 displays all other first-order optic phonons and various combination modes along with their frequency positions. The origin of an unidentified mode assigned by asterisk (*) could not be understood at this time. Further, Raman scattering experiments were performed in various scattering configurations, where a weak E_1(LO) phonon mode was observed with z(x,x)-z scattering configuration, the A_1(TO) mode was observed in both x(y,y)-x and x(z,z)-x scattering configurations and the E_1(TO) mode was observed in both x(y,z)-x and x(y,z)y scattering configurations. The E_2 modes were observed in four different scattering configurations. Figure 2 displays Raman spectra between 520 and 580 cm^{-1} in three different scattering configurations. The assignment of all observed modes and their frequency positions are in good agreement with those reported earlier [2] for wurtzite GaN crystal, which was not bulk, but epitaxially grown crystal.

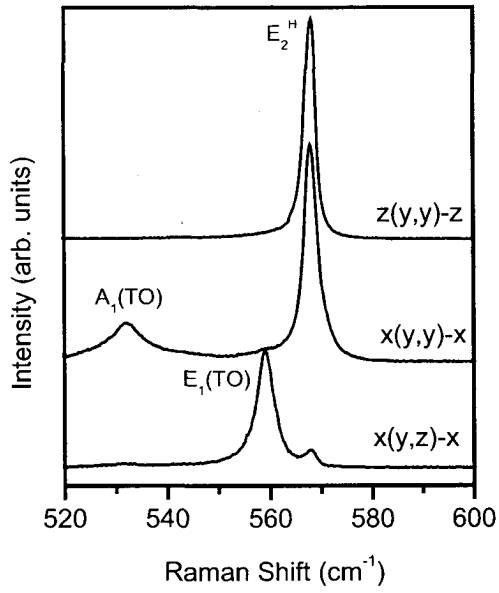

Fig. 1 Some of the Raman spectra in the spectral range of 520 to 580 cm^{-1} from bulk GaN in the indicated scattering configurations.

[1] S. Nakamura, Solid Stat Commun. **102**, 237 (1997).

[2] H. Siegle, G. Kaczmarczyk, L. Filippidis, A. P. Litvinchuk, A. Hoffmann, and C. Thomsen, Phys. Rev. B **55**, 7000 (1997).

Characterization of SiC band-edge absorption properties by free-carrier absorption technique with variable excitation spectrum

P. Grivickas[1]*, V. Grivickas[2], A. Galeckas[1,2] and J. Linnros[1]

1 Department of Microelectronics and Information Technology, Royal Institute of Technology, Electrum 229, SE-16440 Kista-Stockholm, Sweden
2 Institute of Materials Science and Applied Research, Vilnius University, Sauletekio 10, 2054 Vilnius, Lithuania
* Tel. +46 8 752 1345, fax +46 8 752 7782, e-mail: paulius@ele.kth.se

Optical absorption at the edge of the fundamental bandgap is an important parameter for various characterization techniques where excitation effect is employed. In silicon carbide (SiC) optical excitation is relatively weak due to the indirect bandgap nature of this material, and therefore assessment of the band to band absorption coefficient α_{bb} becomes a complicated issue. Conventional methods like transmission or photo-thermal deflection can detect only the overall absorption of the incident radiation. Such measurements require thick samples, thus high quality but thin SiC epilayers appear to be beyond the sensitivity limits. On the other hand, available bulk SiC samples are usually moderately or heavily doped, making measurements of the intrinsic absorption edge strongly influenced by intra-band transitions of the extrinsic free-carriers. As a consequence, an intrinsic band tail and doping-induced band-gap narrowing in different SiC polytypes are not determined yet.

In this paper we present optically induced free-carrier absorption (FCA) as a sensitive tool to analyze spectral dependencies of the band to band absorption coefficient $\alpha_{bb}(h\nu)$ for photon energies $h\nu$ near and below the indirect band gap. The major advantage of this method is that absorption coefficient α_{bb} could be studied in high-quality low-doped SiC epilayers avoiding interference with the extrinsic free-carrier absorption. Another benefit comes from the fact that the FCA cross-section σ_{eh} for the IR-light used to probe SiC is rather large for a specific polarization [1] allowing the detection of very small absorption coefficients possible. Moreover, a linear relationship between FCA and the injected carrier density in SiC polytypes has been proven over a wide injection range (10^{13}-10^{19} cm^{-3}) and a wide temperature interval. In addition, due to a tight focusing of the probe beam down to a few microns relatively high spatial resolution could be achieved even for thin epilayer samples. The FCA technique with variable excitation spectrum has been already applied to crystalline silicon, where a perfect agreement between the measured and literature reported $\alpha_{bb}(h\nu)$ values has been obtained [2].

In this work, FCA measurements were performed on the high-quality (>500 ns lifetime at room temperature) free-standing 4H and 6H epilayers with extrinsic carriers concentrations of 10^{15} cm^{-3}. Perpendicular pump-probe measurement geometry has been applied as shown in the insert of Fig. 1. A short exciting laser pulse from a tunable optical-parametric-oscillator (OPO) penetrates the sample from the narrow facet. Excited free-carriers concentration is detected by the FCA of the 1.3 μm probe beam aligned parallel to the excitation surface. The advantage of such configuration is that both **E** || **c** and **E** ⊥ **c** measurements can be performed while the polarization of the excitation light is rotated. The amplitude of the FCA signal is proportional to the photo-generated carrier density according to the relation: $\Delta\alpha_{FCA} = \sigma_{eh}\Delta n = I_0 \cdot (1\text{-}R) \cdot \alpha_{bb}(h\nu) \cdot \exp(\alpha_{tot}(h\nu) \cdot x)$, where Δn is concentration of the excited carriers, I_0 - density of the incident phonons, R - reflectivity and x - the distance from the excited facet. The total absorption is $\alpha_{tot}(h\nu) = \alpha_{bb}(h\nu) + \alpha_{fc}(h\nu)$, where $\alpha_{fc}(h\nu)$ stands for an extrinsic free-carrier absorption and is assumed to be negligible in the vicinity of

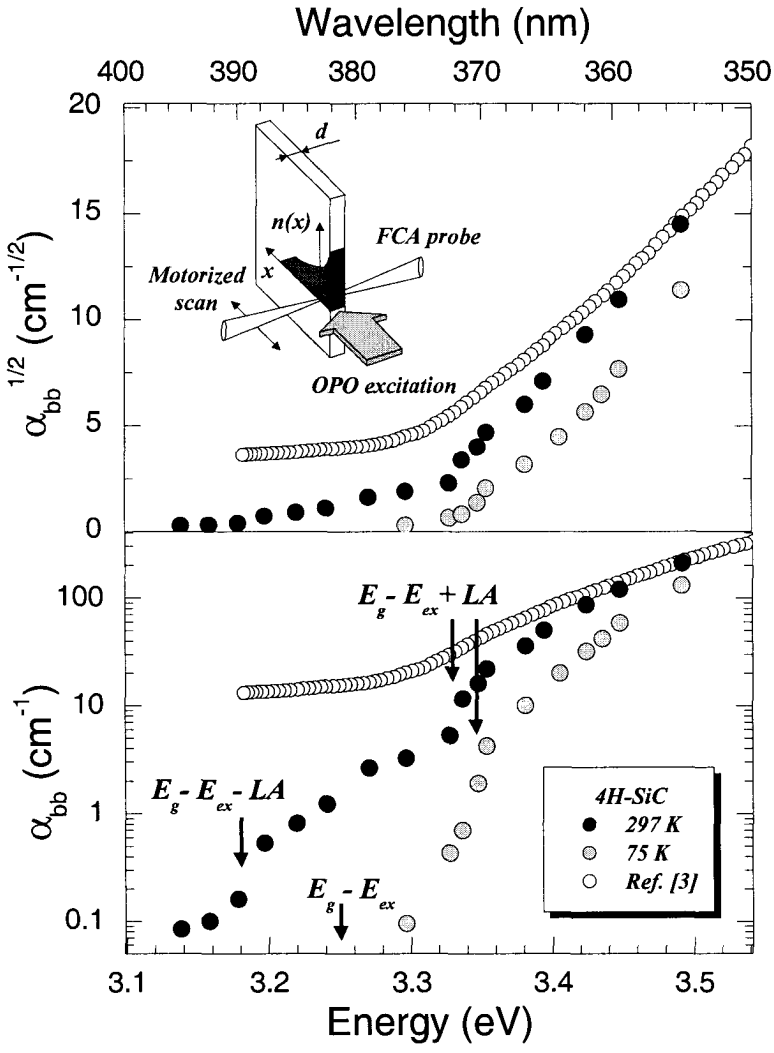

Fig. 1. Band to band absorption coefficient α_{bb} versus the excitation energy in 4H-SiC at 75 and 297 K. Inset - measurement geometry.

the injected facet, since $[\alpha_{tot}(h\nu)\cdot x] << 1$. More detailed considerations about the technique are provided in Ref. [2].

Fig. 1 shows the measured $\alpha_{bb}(h\nu)$ dependencies in 4H-SiC for **E** ⊥ **c** at the temperatures 75 and 297 K. In the high-energy range (>3.35 eV) the absolute α_{bb} values were extracted from the exponential penetration slopes. The low energy part of the spectra was determined in the vicinity of the excitation facet where the FCA amplitude $\Delta\alpha_{FCA}$ was calibrated with the high-energy α_{bb} values. Our data at high energies are comparable to those obtained by conventional transmission measurements for *n*-type 4H SiC boule slice with a doping concentration of about 10^{16} cm^{-3} [3] (open symbols in the plot). However, the low-energy side of these published spectra exhibits an interference with extrinsic free-carrier absorption due to the relatively high doping. In the same region around the band edge we are able to detect nearly two orders of magnitude smaller α_{bb} values. Despite the relatively low spectral resolution in our measurement (around 25 meV) the main sharp feature in our spectra at 75 K suggests the absorption step to the 76 meV *LA* phonon (loger arrow near the E_g–E_{ex}+*LA* indication). This most pronounce singularity was as well observed in the differential absorption spectra at 2 K [4]. At room temperature a wide tail rises up in the low energy side of the spectra and we assign this feature to the emission of the same *LA* phonons. Thus the middle point between two step features (indicated by E_g–E_{ex}+*LA* and E_g–E_{ex}-*LA* with short arrows) could be estimated as the excitonic band gap E_g-E_{ex} = 3.255 eV of the 4H-SiC which is in good agreement with a value extrapolated from PL measurement [5].

References:

[1] V. Grivickas, A. Galeckas, P. Grivickas, J. Linnros, Mat. Sci. Forum 338-342 (2000) 555.
[2] V. Grivickas, Sol. State Commun. 108 (1998) 561, (spectral measurements – unpublished).
[3] S. G. Sridhara et al. Mat. Sci. Engin. B61-62 (1999) 229, J. Appl. Phys. 84 (1998) 2963.
[4] S. G. Sridhara et al. Mat. Sci. Forum 338-342 (2000) 567.
[5] A. Itoh, et al. Jpn. J. Appl. Phys. 35 (1996) 4373.